Journal of Catalysis 347 (2017) 148–156

Contents lists available at ScienceDirect

Journal of Catalysis

journal homepage: www.elsevier.com/locate/jcat

Au^0–Au^{3+} bifunctional site mediated enhanced catalytic activity of Au/ZnO composite in diesel particulate matter oxidation

Grisel Corro [a,*], Surinam Cebada [a], Umapada Pal [b], Jose Luis García Fierro [c]

[a] Instituto de Ciencias, Benemérita Universidad Autónoma de Puebla, 4 sur 104, 72000 Puebla, Mexico
[b] Instituto de Física, Benemérita Universidad Autónoma de Puebla, Apdo. Postal J-48, 72570 Puebla, Mexico
[c] Instituto de Catálisis y Petroleoquímica, Cantoblanco, 28049 Madrid, Spain

ARTICLE INFO

Article history:
Received 19 December 2016
Revised 16 January 2017
Accepted 21 January 2017

Keywords:
Au/ZnO composite catalyst
Diesel particulate matter oxidation
Au^0-Au^{3+} catalytic site
Diesel combustion

ABSTRACT

Hydrogen-reduced air-calcined 1%Au/ZnO composite synthesized by gold impregnation in ZnO has been utilized as catalyst for diesel particulate matter (DPM) oxidation. The catalyst was characterized by UV-vis optical absorption, X-ray photoelectron spectroscopy and transmission electronic microscopy. The composite catalyst showed excellent activity for the oxidation of DPM at temperature as low as 230 °C. The activity of the catalyst does not change up to 6 oxidation cycles. The high catalytic activity of the composite has been attributed to the formation of stable Au^0–Au^{3+} bifunctional catalytic sites at the gold-ZnO interface, which enhances the contact efficiency of solid particulate matter on Au^{3+} and the generation of superoxide species on Au^0. The high stability of the bifunctional Au^0-Au^{3+} sites is associated with the electronic interactions between gold and n-type semiconductor ZnO at their interface.

1. Introduction

Particulate matters (PM), containing mainly the soot emitted from diesel engines have caused acute human health and environmental problems [1]. Wall flow filters are commonly employed in diesel engine exhausts to trap these soot particulates. However, to keep the backpressure of the engine low, the filter needs frequent regeneration by burning the trapped soot at high temperatures, which often damage the filter.

Diesel particle traps with different designs can be used for diesel particulate matter (DPM) removal from gas streams [2,3]. Once the DPM is collected on a filter, different regeneration strategies can be applied. The thermal combustion is usually performed above 450 °C. The use of a catalyst is the key to lower the ignition temperature [4]. Among the available technologies for filter regeneration, there is PSA system, in which a Ce fuel additive leads to the formation of CeO_2 particles well embedded into the DPM structure, lowering its ignition temperature. Although this system works satisfactorily, fuel penalty and high investment cost are its main drawbacks [5]. On the other hand, the Continuously-Regenerating–Trap (CRT system by Johnson Matthey) that consists of a wall-flow trap with an upstream flow through a platinum-group-metal catalyst converts NO to NO_2, which rapidly reacts with trapped DPM. The system oxidizes DPM at temperatures as low as 220 °C [6].

The key challenge of this technology is to develop a catalyst that can accelerate particulate matter oxidation at temperatures as low as possible [7–9].

The catalytic activity of a material for diesel particulate matter (DPM) oxidation is affected by two factors: the contact efficiency between solid particles and the catalyst surface, and the intrinsic activity of the catalyst [10–17].

For a long time, gold did not attract much attention in catalyst research and chemical engineering as it is catalytically much less active than the platinum group metals due to its $5d^{10}$ electronic configuration. In the absence of support material, H_2, CO and O_2 are not adsorbed on pure gold surfaces. On the other hand, hydrocarbons interact only weakly with gold surfaces [18]. The intrinsic inertness of gold could be overcome successfully by dispersing over support surface as small nanoparticles.

Downsizing the dimension of particles however, also affects their electronic properties. For gold nanoparticles grown by vapor deposition under ultrahigh vacuum on single crystalline TiO_2 (1 1 0) surfaces, scanning tunneling spectroscopy revealed a higher band gap (HOMO-LUMO gap) for particles smaller than 4 nm, which increases further with size reduction, giving rise a non-metallic character to these fine particles [19]. The result suggests that if the metal-mediated oxidation depends on the nature of metal, significant changes in catalytic properties should be

* Corresponding author.
E-mail addresses: griselda.corro@correo.buap.mx (G. Corro), upal@ifuap.buap.mx (U. Pal), jlgfierro@icp.csis.es (J.L.G. Fierro).

http://dx.doi.org/10.1016/j.jcat.2017.01.011
0021-9517/

observed with the electronic change (or charge distribution) of metal nanostructures. One powerful method for determining the electronic state of metal is X-ray photoelectron spectroscopy (XPS). The electronic properties of metal nanoparticles also differ markedly from their bulk counterparts due to quantum size effects [20]. The essential issue of these phenomena is that in nanometric particles, the conduction electron band is not a continuum as in the bulk metal, but splits into discrete energy levels.

Supporting gold nanoparticles as active components is an attractive choice to enhance the intrinsic catalytic performance of oxidation catalysts, because they promote adsorption-activation of molecular oxygen and increase the amount of active oxygen species ($O_2^{\&-}$) over the catalyst surface [21–32]. Gold nanoparticles dispersed on metal oxides have been applied to a number of catalytic reactions including complete oxidation of hydrocarbons, hydrogenation, NO reduction, and water gas shift reactions [33–35].

The efficiency of supported Au nanoparticles depends on their size and shape [36], the nature of the support [37], the oxidation state of the active gold species (Au^0, Au^{1+} or Au^{3+}) [38], the gold species-support interactions, and the oxygen supply pathways [39]. It is commonly accepted that activation of O_2 is the most critical step in catalytic oxidation reactions involving gold. The reactivity of gold clusters with O_2 is important for understanding their remarkable catalytic effects. One of the reported reasons of the chemisorption and activation of O_2 on Au-based catalysts is the so-called metal-support interactions. These include electronic interactions between the components (metal and the support) [40], stabilization of certain shapes or sizes of the particle [41], strong metal-support interactions [42] or the stabilization of oxidized active phases by the support [43]. Wei et al. [44] have successfully synthesized three-dimensionally ordered macroporous $Au/Ce_{1-x}Zr_xO_2$ catalysts which, with the assistance of NOx could decrease the ignition temperature of diesel soot as low as to 250 °C even in loose contact conditions. However, a poor thermal stability of supported Au based catalysts for soot oxidation was reported. Indeed, gold-based catalysts have been commercialized for diesel engines (e.g. Nanostellar Inc.) for the control of CO and HC in their exhausts [45]. However, an exact mechanism of gold-mediated catalysis has not been fully understood, especially for the reactions associated with particulate matters.

In general, the catalysts studied for DPM oxidation have smaller pore sizes (>10 nm) than the size of DPM particles, whose diameter varies from 20 nm to 1 μm. Thus, it is difficult for the DPM particles to enter into the inner pores of these catalysts with high surface area [46–48]. Therefore, the contact area and the exposed active sites are limited, which affect the performance of the catalyst.

In the present work, we present a 1%Au/ZnO composite, which can act as efficient catalyst for DPM oxidation at low temperature. The catalyst was prepared by impregnation of gold ion solution in ZnO particles of a very low specific surface area. We used this support due to its bigger average pore size (>50 nm), which could permit solid reactant to enter the inner pores of the catalyst, with easy to transport and diffuse. Consequently, the effective contact area between the DPM and the catalyst would increase.

The structural and electronic properties of the catalyst were studied utilizing X-ray photoelectron spectroscopy (XPS), UV-vis diffuse reflectance spectroscopy (DRS) and transmission electronic microscopy (TEM) techniques. The catalytic behavior of the composite in DPM oxidation in 25–600 °C temperature range has been correlated with its physicochemical properties, considering the interactions of active and non-active species such as Au^0, Au^{1+}, and Au^{3+} with oxygen and DPM, along with the interactions between Au and the ZnO support.

2. Experimental section

2.1. Catalysts

2.1.1. Catalyst preparation

ZnO powders obtained from Merck, Germany (99.9%), were impregnated with appropriate amount of aqueous $NaAuCl_4$ (Aldrich 99.99%) solution to obtain a nominal 1 wt% Au/ZnO mixture. The suspension was magnetically stirred at room temperature for 1 h, after which the catalyst was recovered by filtration, and washed thoroughly to remove soluble sodium, chlorine, and other unreacted species (if any), and dried at 120 °C overnight. After drying, the resulting powder was reduced under pure H_2 using a feed volume flow rate of 80 ml min^{-1} at 450 °C for 4 h. The temperature of the furnace was increased at the rate of 10 °C min^{-1}. After cooling down to room temperature (25 °C) under H_2 flow, the sample was purged with air for 30 min. The catalyst was then calcined under air using a feed volume flow rate of 100 ml min^{-1} at 600 °C for 4 h. After cooling down to room temperature (25 °C) the catalyst was stored in dry conditions, after which it is called 1%Au/ZnO. A ZnO sample, without $NaAuCl_4$ solution impregnation was prepared in the same way to use as the reference.

2.1.2. Catalyst characterization

The loadings of Au and Na species in the catalyst were determined using a Shimadzu AA-7000 atomic absorption spectrophotometer, with hollow Au and Na cathode lamps and a deuterium background corrector at respective wavelengths using an air-acetylene flame. The lamp current was set to 10 mA.

A Quantachrome Nova-1000 sorptometer was used to measure the N_2 adsorption-desorption isotherms of the catalysts. Specific surface area (S_g) of the samples was estimated from their N_2 physisorptions at 77 K, using BET analysis. The samples (1 g each) were degassed at 400 °C for 2 h before recording their adsorption-desorption isotherms. After cooling to room temperature (25 °C), the isotherms were recorded in the pressure range 0.0–6.6 kPa. The technique of back extrapolation of the linear portion of the isotherms to zero equilibrium pressure was used to determine the saturation uptake.

The diffuse reflectance spectra (DRS) of the catalysts before and after 6 particulate matter oxidation cycles were measured on dry-pressed disks (~15 mm diameter) using a Shimadzu UV-vis spectrophotometer equipped with an integrating sphere, and $BaSO_4$ as standard reflectance sample. The crystallinity and structural phase of the samples were verified through powder X-ray diffraction (XRD), using the CuK_α radiation (λ = 1.5406 Å) of a Bruker D8 Discover diffractometer.

X-ray photoelectron spectra (XPS) were recorded on freshly prepared 1%Au/ZnO catalyst and after its 6th particulate matter oxidation cycle, using an Escalab 200R electron spectrometer equipped with a hemispherical analyzer, operating in a constant pass energy mode. Monochromatic MgK_α emission ($h\nu$ = 1253.6 eV) from the X-ray tube operating at 10 mA and 12 kV was utilized for recording XPS spectra of the samples. Different energy regions of interest of the photoelectrons were scanned a number of times in order to get good signal-to-noise ratios. The intensities of the emission peaks were estimated by determining the integral of each peak after subtracting an S-shaped background and fitting the experimental peak to Lorentzian/Gaussian curves (80%L/20%G). The peak positions of the elements were corrected utilizing the position of C*1s* peak coming from adventitious carbon appeared at 284.9 ± 0.2 eV.

TEM images of the fresh 1%Au/ZnO and after 6 oxidation cycles were obtained in a JEM 2100F microscope fitted with an INCA

X-sight (Oxford Instruments) energy dispersive X-ray spectroscope (EDX), operating at 200 kV accelerating voltage.

2.2. Generation of diesel particulate matter

The particulate matter used in this study was generated by burning pure Mexican diesel acquired from the market in a glass vessel, under controlled air flow as described in Fig. 1. In this study, the term 'particulate matter' is used to refer both the soluble and insoluble (carbon) fractions of the diesel-emission.

The emission from the exhaust of the vessel was directed through a 20 cm long pipework to the catalyst sample (200 mg) placed inside a tubular quartz reactor (inner diameter 10 mm) in a programmable furnace. The process was performed using an air feed volume flow rate of 100 cm^3 min^{-1}. The diesel particulate matter (DPM) generated from the exhaust of the vessel was accumulated on the catalyst in the tubular reactor. After 1 h of diesel combustion, the total amount of DPM retained by the catalyst in the blank experiment was about 8.45 mg (measured using a Shimadzu AX200 balance), attaining a DPM/catalyst mass ratio of 0.042. The amount of DPM retained by the catalyst was measured after 3 accumulation processes before proceeding with its temperature programmed oxidation. The DPM mass accumulated was rather constant and about 8.4 ± 0.5 mg.

In Fig. 2, pictures (magnified 400×) of 1%Au/ZnO before (a) and after (b) DPM deposition can be observed. It is interesting to note a homogeneous mixture of the DPM and the catalyst after deposition.

The contact between DPM and the catalyst during DPM accumulation was considered similar to the contact between the DPM generated from a real diesel engine and the catalyst used in a particulate filter. However, in order to compare the reactivity of 1%Au/ZnO for the DPM (formed by soluble and insoluble carbon) oxidation with other literature results obtained using synthetic soot [49,50,48,13,51–56], we performed additional experiments using carbon-black from Degussa (Printex-U, with 92.0% C, 3.5% O, 0.3% N, 0.3% S and 3.9% other). The catalyst (200 mg) and soot (2 mg) were mixed with a spatula in the so-called loose contact mode [57]. A picture of the mixture (magnified 400×) can be seen in Fig. 2(c). The mixture was placed inside the tubular quartz reactor (inner diameter 10 mm) in the programmable furnace. The process was performed using an air feed volume flow rate of 100 cm^3 min^{-1}.

Organic functional groups in the DPM synthesized in this investigation and in the Printex-U carbon-black were analyzed using a Bruker FT-IR spectrometer (Vertex 70) in the 800–4000 cm^{-1} spectral range. A thin, uniform KBr pellet prepared with 0.2 wt% of the samples was used for recording the FT-IR spectra.

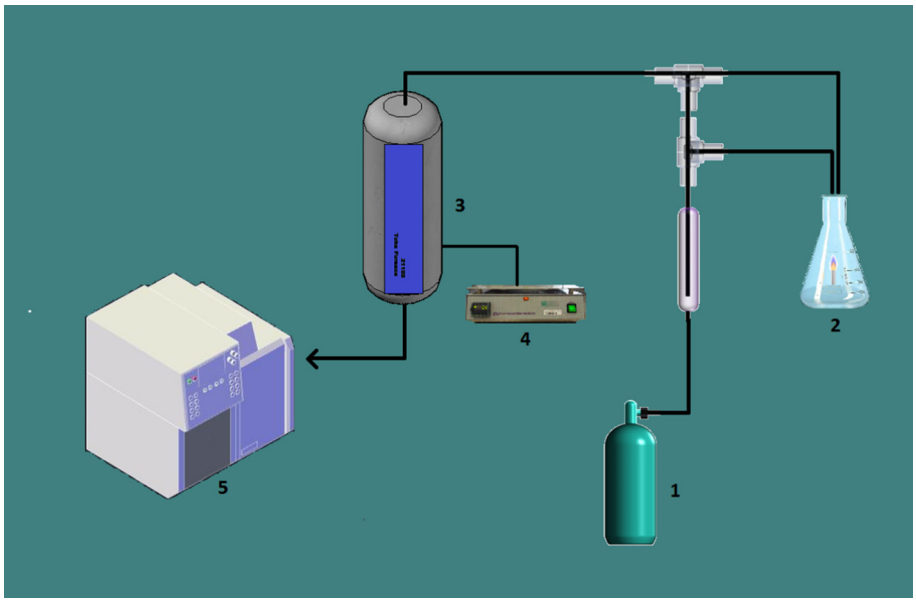

Fig. 1. Schematic diagram of the system used for monitoring the combustion process. 1: Air; 2: Diesel burner; 3: Reactor; 4: Temperature controller; 5: Gas chromatograph.

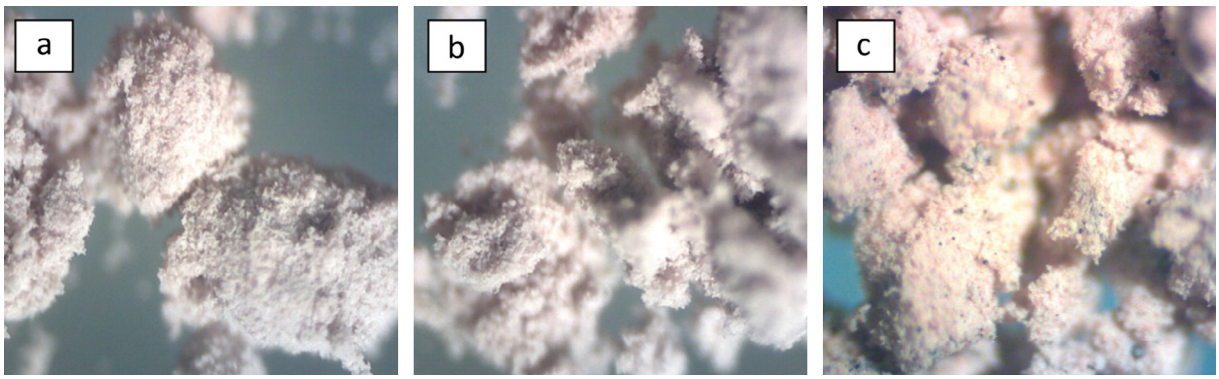

Fig. 2. Photographs of 1%Au/ZnO catalyst (a): before; (b): after DPM deposition and (c): mixture of 1%Au/ZnO and carbon-black (Printex-U).

2.3. Particulate matter oxidation through programmed temperature experiments

After the accumulation of DPM over the catalyst surface (or after placing the catalyst/carbon-black in the reactor), air was purged for 15 min to remove weakly attached combustion products. The air (20 vol% of O_2 and 80 vol% of N_2) flow rate was maintained at 100 cm^3 min^{-1}. The mixture was then heated from room temperature (25 °C) to 600 °C at the rate of 5 °C min^{-1}. A thermocouple was inserted into the DPM-catalyst mixture to monitor its temperature along with the exothermic heat of the DPM oxidation. The emissions from the reactor were analyzed every 5 min through a computer programmed Shimadzu gas chromatograph provided with a thermo-conductivity detector (TCD) to monitor the CO_2 evolution at different temperatures. The chromatograph was fitted with a Porapak column to analyze CO_2 evolutions as a function of the temperature of the particulate matter-catalyst mixture. The process comprising particulate matter accumulation on the catalyst at room temperature (during 1 h), its subsequent oxidation at high temperature, and then cooling down to 25 °C is called a cycle. The duration of each cycle was about 2.5 h. After the first cycle, five similar cycles were performed over the same 1%Au/ZnO sample. The same process was performed for the mixture catalyst/carbon-black placed in the reactor. In order to determine the catalyst effect, an uncatalyzed particulate matter oxidation cycle was performed over only quartz wool at fixed temperatures between 25 and 800 °C.

3. Results and discussion

3.1. Characterization of the catalysts

3.1.1. Surface area analysis and Au and Na loading determinations

The specific surface area of the catalysts before and after utilization in oxidation cycles was estimated from their N_2 adsorption-desorption isotherms recorded at 77 K. Obtained results are summarized in Table 1. All the freshly prepared catalysts revealed very low specific surface area, which remained constant after their use in DPM oxidation cycles. From Table 1, it can be seen that the estimated gold and sodium loadings (AAS results) in the catalyst were 1.03% and 0.0005%, respectively. Such a low concentration of Na in the catalyst is expected to have no influence in the performance of the catalyst.

3.1.2. UV-vis characterization of the catalysts

Fig. 3 shows the UV-vis diffuse reflectance spectra (DRS) of ZnO and 1%Au/ZnO, before and after their use in DPM oxidation cycles. The absorption spectrum (spectrum c) of the 1%Au/ZnO sample before its use in DPM oxidation revealed two bands. The first band appeared between 450 and 650 nm with maximum around 562 nm corresponding to the surface plasmon resonance (SPR) of Au nanoparticles [58]. The second band is observed with onset around 400 nm, which is close to the absorption edge of ZnO semiconductor (spectrum a) [59]. On the other hand, in the figure, it can be seen that there are not differences between the absorption spectra of the catalyst before (spectrum c) and after DPM oxidation (spectrum d). This result suggests that the electronic state of Au particles in 1%Au/ZnO remained the same, even after six soot oxidation cycles.

3.1.3. XPS characterization of the catalysts

The catalytic performance of a material in oxidation reaction is frequently correlated with its capability to activate oxygen. To determine the possible interactions between the catalyst and oxygen, the electronic properties of the gold supported over ZnO were studied by XPS before and after using the catalyst (1%Au/ZnO) in oxidation cycles. The results are presented in Fig. 4 and Table 2. The XPS spectrum of the freshly prepared 1%Au/ZnO catalyst revealed Au $4f_{7/2}$ emission band with three components located around 83.4, 85.6, and 88.0 eV, corresponding to Au^0, Au^{1+}, and Au^{3+} states, respectively (Fig. 4). On the other hand, the catalyst after utilization in 6 DPM oxidation cycles, revealed similar three fold Au $4f_{7/2}$ emission and the positions of the component bands (i.e. their binding energies) remained the same as that of the unused catalyst. In Table 2, it can be seen that the content of gold in Au^0, Au^{1+}, and Au^{3+} states remained the same in the catalyst after using in oxidation cycles. These results indicate that the electronic state of Au particles in 1%Au/ZnO remained the same, even after six soot oxidation cycles. On the other hand, the Au/Zn atomic ratio value at the surface of the catalyst remained the same after using it in 6 DPM oxidation cycles. These results show the high stability of the catalyst for the oxidation cycles.

3.1.4. TEM images of the catalysts

Representative TEM images and Au particle size distribution of 1%Au/ZnO before and after the DPM oxidation cycles are presented in Fig. 5. The Au particles can be seen as dark contrasts on the surface of ZnO particles. Average diameter of the Au nanoparticles estimated from their size distribution histograms was 89.3 nm

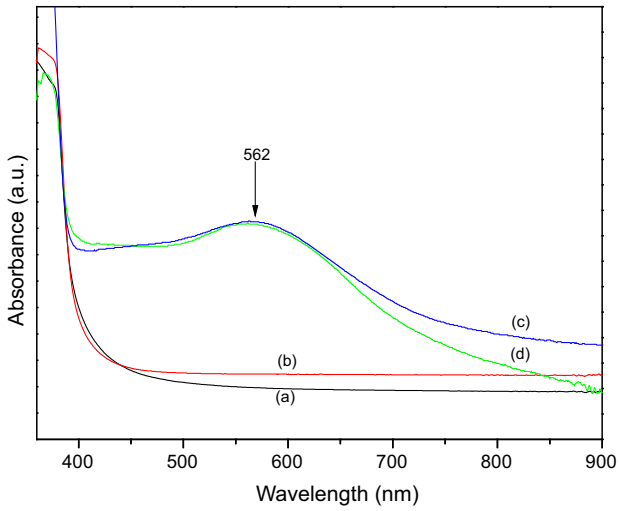

Fig. 3. UV-vis absorption spectra of the (a) ZnO before using in oxidation cycles; (a) ZnO after oxidation cycles; (c) 1%Au/ZnO before using in oxidation cycles; (d) 1%Au/ZnO after 6 oxidation cycles.

Table 1
Au and Na loading, and estimated specific surface area of the catalysts before and after their utilization in particulate matter oxidation cycles.

Catalyst	Metal loading (%)		Specific surface area (m^2 g^{-1})	
	Au	Na	Fresh sample	After oxidation cycles
ZnO	–	–	4.78	4.62[a]
1%Au/ZnO	1.03	0.0005	3.93	3.69

[a] After 1st cycle.

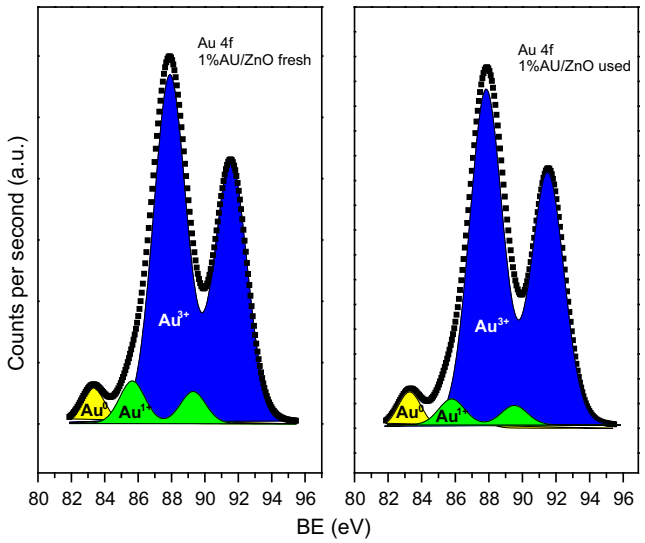

Fig. 4. XPS spectra of 1% Au/ZnO before and after 6 particulate matter oxidation cycles.

Table 2
Binding energy positions of the components and Au/Zn atomic ratio at the surface of the catalysts before and after using them in 6 diesel particulate matter oxidation cycles. The % peak area of Au^0, Au^{1+}, and Au^{3+} components is presented in parentheses.

Catalyst	Au $4f_{7/2}$ (eV)	Zn$2p_{3/2}$ (eV)	O*1s* (eV)	Au/Zn atomic ratio
1%Au/ZnO before particulate matter oxidation	83.4 (7)85.6 (9) 88.0 (84)	1021.5	530.4	0.189
1%Au/ZnO after particulate matter oxidation	83.3 (6)85.6 (8) 87.9 (86)	1021.5	530.3	0.181

and 90.5 nm for the fresh catalyst and after its use in oxidation cycles, respectively. The results show that during the 6 DPM oxidation cycles, the Au particle size distribution remained the same. During preparation, the catalyst was first reduced at 450 °C and then calcined at 600 °C. Both temperatures were higher than the Tammann temperature of gold (395 °C). Such high temperature pretreatments to the catalyst lead to the sintering of already formed gold particles over catalyst surface, and increase their size (around 90 nm) before their use in catalytic reactions. It is worth noting that most of the reported gold catalysts contain smaller particles [60].

From Fig. 5, we can see that the gold particles are hemispherical in shape and they are attached to the support through their flat plane with a specific crystal orientation with respect to the support. The interfaces between Au and ZnO thus appear to be in tight contact, exhibiting specific crystal orientation. This fact strongly suggests that Au atoms are at the metal-support interface, with electronically different characters compared to the other atoms of the nanoparticle. The images revealed no traces of carbon or other particulate matter after 6 DPM oxidation cycles. These results are consistent with UV-vis and XPS results discussed in the previous sections.

3.2. Diesel particulate matter oxidation over the catalysts

3.2.1. Diesel particulate matter oxidation over ZnO

The DPM oxidation activity of ZnO was measured for the first oxidation cycle, in the temperature range 25–600 °C (results not shown). Only a very small amount of CO_2 was detected at about 590 °C, indicating that the total oxidation of DPM was not achieved.

As the UV-vis absorption spectra of ZnO (Fig. 3) before and after its use in the particulate matter oxidation cycle remained rather unchanged, it can be considered that the electronic structure of ZnO remained the same even after the DPM oxidation cycle.

3.2.2. Diesel particulate matter oxidation over 1%Au/ZnO

CO generated during the 6 DPM oxidation cycles was not detected in the studied temperature range, probably due to the strong oxidation activity of 1%Au/ZnO, which might have oxidized CO at an oxidation rate higher than the CO generation rate. Indeed, Haruta et al. [35] demonstrated that supported Au catalysts are very active for CO oxidation at temperatures "as low as 0 °C."

Fig. 6 shows the temperature evolution of CO_2 during the 6 DPM cycles over the 1%Au/ZnO catalyst. In all the six CO_2 evolution curves, there appeared a sharp signal through 200–300 °C, peaking at 230 °C, indicating that the highest DPM oxidation temperature (T_{max}) remains the same from cycle to cycle. The unaltered position of T_{max} would mean that during the 6 oxidation cycles, the stoichiometry and the electronic structure of the catalyst remained unaltered.

In order to discard a possible deactivation of the catalyst due to high concentrations of CO_2 and water which are present in a real diesel engine exhaust gas, we performed the following experiment. The combustion emissions (comprising produced CO_2, CO, HC, NO_x, and H_2O) from the exhaust of the vessel (used in this investigation) were directed to a catalyst sample in the tubular reactor, for 8 h at 300 °C, after which the temperature was lowered to 25 °C and a new DPM deposition followed by its TPO was performed. In Fig. 6 (7th cycle) it can be seen that the CO_2 evolution profile and the T_{max} of this cycle remained the same as that of the process performed with air. The results indicate that CO_2 and H_2O do not affect the activity of 1%Au/ZnO catalyst, in contrary to the results reported by Goguet et al. in the study of water gas shift reaction catalyzed by Au/$CeZrO_4$ [61].

In order to compare our results with those reported in the literature in which synthetic soot (in loose mode) was used to investigate the catalytic activity for soot oxidation, we performed an additional experiment using carbon-black (Printex-U) to measure the oxidation activity of 1%Au/ZnO in loose contact mode (Fig. 7). This result indicates a high activity of 1%Au/ZnO for carbon-black oxidation. However, the T_{max} determined for this reaction (350 °C) is higher than the T_{max} measured (~230 °C) for the DPM generated by direct diesel burning.

Fig. 8(a) shows the FT-IR spectrum of DPM synthesized in this investigation. Principal characteristic peaks revealed in this spectrum correspond to the C—H asymmetric and symmetric stretching of aliphatic groups at 2954 cm^{-1}, 2920 cm^{-1} and 2854 cm^{-1}; C—O stretching of carbonyl groups at 1711 cm^{-1}; C=C stretching of aromatics and alkenes at 1548 cm^{-1}; and conventional coke at 1462 cm^{-1} [62,63]. The signal at about 1358 cm^{-1} has been observed in graphite, carbon black and activated carbon [64]. The spectrum shows a broad signal between 1250 and 900 cm^{-1}, which might be the result of several peak overlapping corresponding to C—O stretching (1191 and 1070 cm^{-1}), C—O—C stretching (1121 cm^{-1}), and C—C—O stretching [62]. The signal at around 2360 cm^{-1} corresponds to atmospheric CO_2 adsorbed on the samples.

Now, the FT-IR spectrum of carbon-black (Fig. 8(b)) revealed similar signals at 1735 cm^{-1}, 1548 cm^{-1}, 1459 cm^{-1}, and 1359 cm^{-1}. However, the signals corresponding to aliphatic groups (between 3000 and 2750 cm^{-1}) and the broad band found in DPM spectrum (between 1250 and 1000 cm^{-1}) corresponding to oxygen containing compounds are not present. From the obtained results,

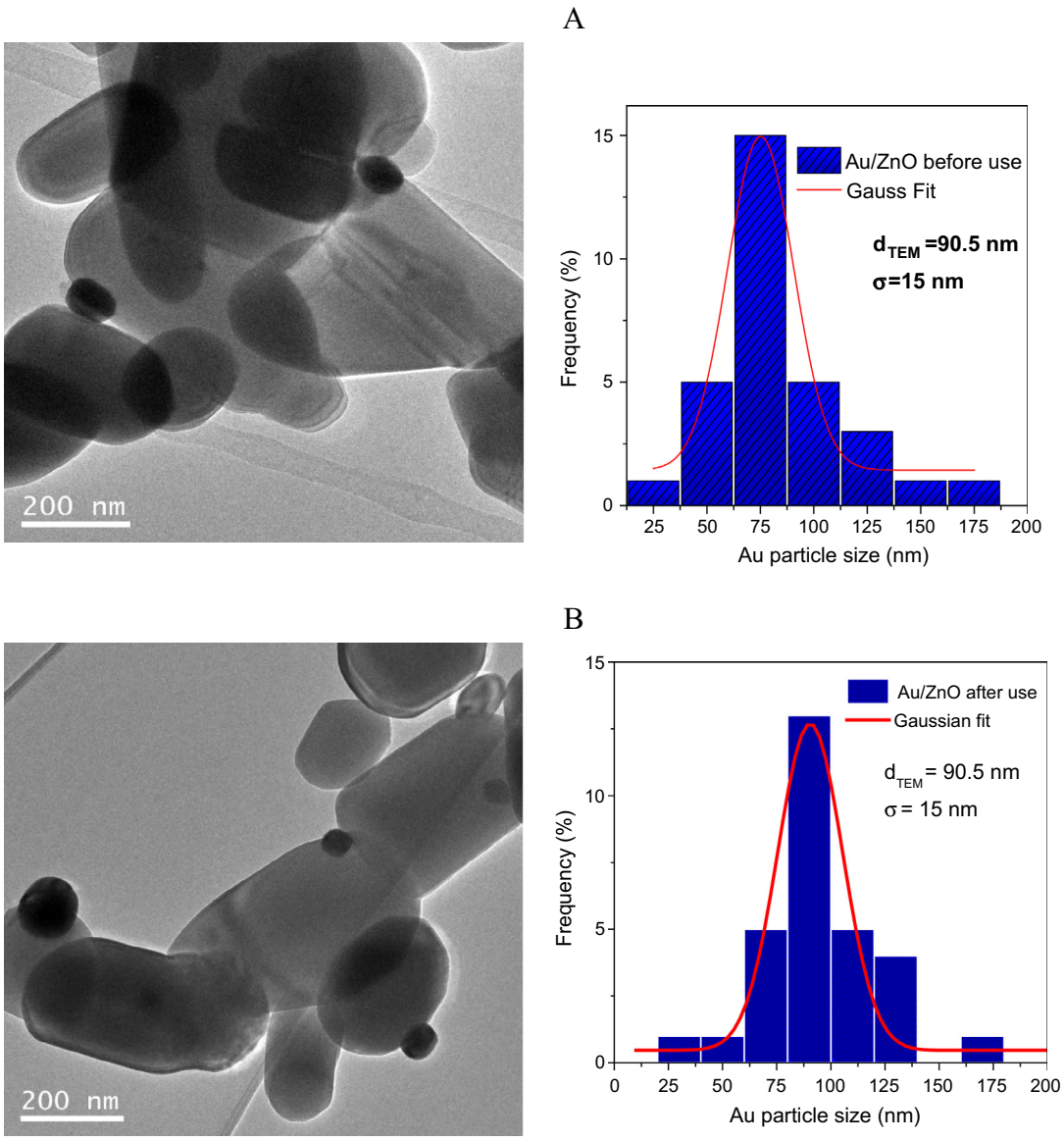

Fig. 5. Typical TEM images and Au particle size distribution of (A) 1%Au/ZnO before DPF oxidation cycles, and (B) 1%Au/ZnO after DPF oxidation cycles.

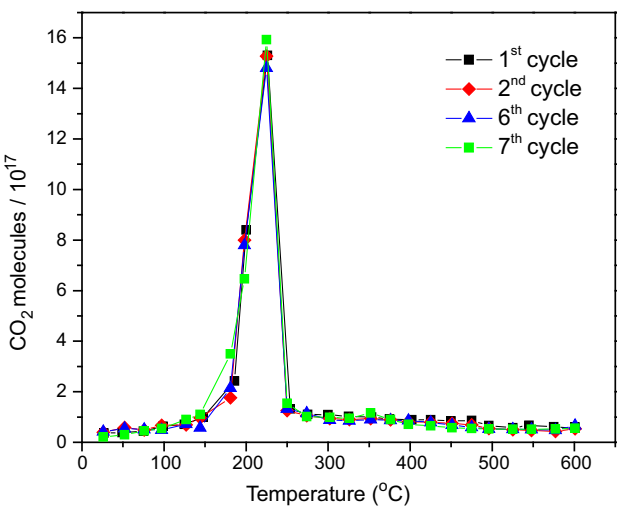

Fig. 6. Evolution of CO_2 as a function of temperature during particulate matter oxidation cycles over 1%Au/ZnO.

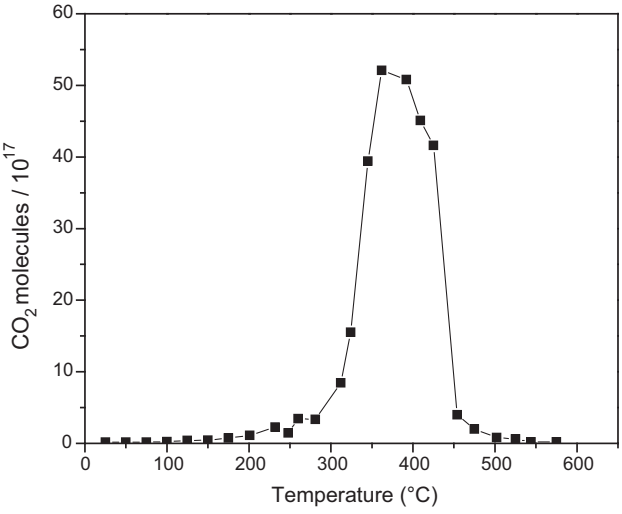

Fig. 7. Evolution of CO_2 as a function of the temperature during carbon-black (Printex-U) oxidation over 1%Au/ZnO.

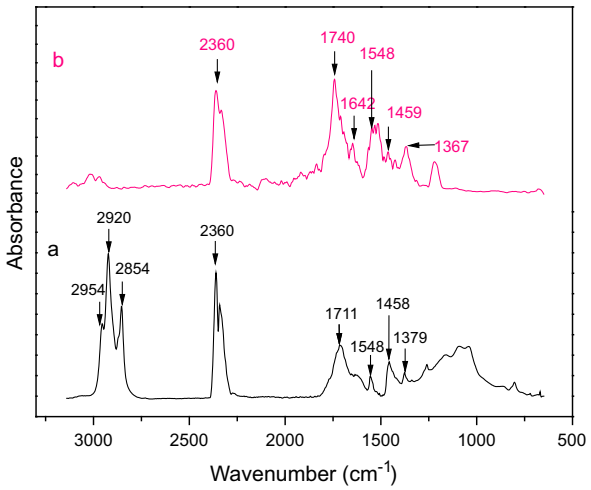

Fig. 8. FTIR spectra of (a) diesel particulate matter sampled from the combustion vessel exhaust, and (b) carbon-black (Printex-U).

it can be concluded that carbon-black (Printex-U) does not contain unburnt hydrocarbons or unburnt oxygen-containing compounds, which may constitute the soluble organic fraction (SOF) in DPM synthesized in this investigation. The composition of this DPM might be similar to the composition of DPM generated by a real diesel engine.

The lower T_{max} measured for DPM oxidation indicates a high amount of DPM in contact with the catalyst, and the transfer of a huge exothermic heat generated during oxidation of the SOF to the neighboring DPM molecules, resulting in low temperature combustion. In the case of carbon-black oxidation, which does not contain the SOF, there is no exothermic heat transfer from SOF combustion, and therefore, higher temperatures will be needed to attain the activation energy for carbon oxidation.

To estimate the catalytic activity of our 1%Au/ZnO composite, CO_2 evolution during particulate matter oxidation in the absence of catalyst was also monitored between 25 and 800 °C. Fig. 10 shows the effect of temperature on DPM oxidation, deposited on quartz wool. As can be seen, only one signal of CO_2 evolution is revealed between 550 and 800 °C, peaked at about 735 °C. Only a very small amount of CO_2 could be detected during the DPM oxidation reaction at temperatures between 25 and 600 °C. At 800 °C, no CO_2 signal was detected, suggesting that the total DPM oxidation was achieved at this temperature. The total area under the CO_2 evolution curve between 25 and 800 °C, $[CO_2]_{Ref}$, was considered as a measure of the maximum amount of carbon in the particulate matter that can be oxidized, generated from the exhaust gas of the vessel and accumulated for 1 h. We define the Relative Catalytic Activity of the catalyst as the ratio of $[CO_2]$ evolved during the catalytic process and the same in the absence of the catalyst (using only quartz wool) as follows:

$$\text{Relative Catalytic Activity} = \frac{[CO_2]_{Cat}}{[CO_2]_{Ref}},$$

where $[CO_2]_{Cat}$ is the area under CO_2 evolution curve (between 25 °C and 600 °C) during particulate matter oxidation over the catalyst, and $[CO_2]_{Ref}$ is the area under CO_2 evolution curve during particulate matter oxidation over quartz wool. The $[CO_2]_{Cat}$ and calculated catalytic efficiency values for the 1%Au/ZnO catalyst for different oxidation cycles have been presented in Table 3. The results obtained from the catalytic evaluation of 1%Au/ZnO composite indicate clearly that the catalyst remains active even after six cycles of particulate matter oxidation, and the oxidation temperature remains as low as 230 °C.

Table 3
CO_2 evolution and estimated relative activity of the composite catalyst for the 1st, 2nd, and 6th oxidation cycles of DPM oxidation.

Catalyst	Intensity of CO_2 evolution (10^{18} molecules)			Relative catalyst activity		
	1st	2nd	6th	1st	2nd	6th
Quartz wool	726					
1%Au/ZnO	720	722	723	0.99	0.99	0.99

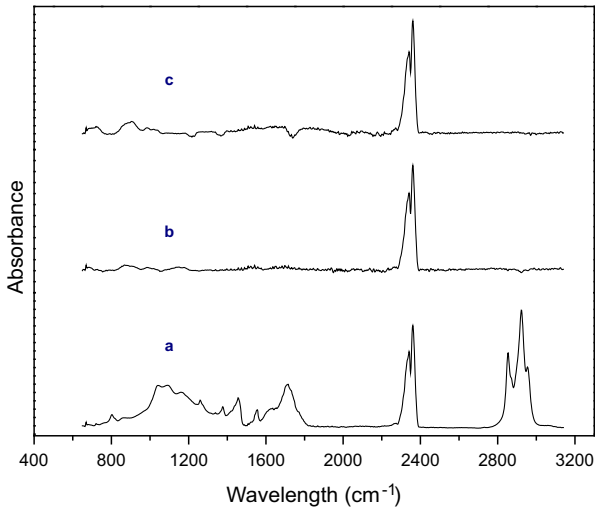

Fig. 9. FTIR spectra of (a) diesel particulate matter sample collected from the combustion vessel exhaust, (b) 1%Au/ZnO after DPF oxidation cycles, and (c) 1%Au/ZnO before DPF oxidation cycles.

The results presented in Table 3 indicate that the total charge of soot deposited in each oxidation cycle was fully oxidized. This observation is supported by the FTIR spectra of the catalyst before and after the oxidation cycles, presented in Fig. 9. The FTIR results show that no carbon traces remained in the catalyst after the oxidation cycles. In addition, the TEM images (Fig. 5) of the catalyst did not reveal any carbon or other particulate matter trace after its use in oxidation cycles.

3.3. Mechanistic considerations of diesel particulate matter oxidation over hydrogen reduced 1%Au/ZnO

XPS analysis of the catalyst used for six particulate matter oxidation cycles revealed the presence of Au^0 at the catalyst surface despite the strong oxidation conditions of the reaction. As the work function of Au (5.3 eV) is higher than that of ZnO (3.9–4.9 eV), an electronic transfer might have occurred at the Au/ZnO interface increasing the stability of Au^0 sites, preventing its oxidation to $Au^{\delta+}$. Moreover, ZnO being an n-type semiconductor, is capable of transferring electrons to the Au core, stabilizing the metallic gold state at the metal-support interface.

Therefore, to explain the exceptional high activity at low temperature of 1%Au/ZnO for the diesel particulate matter oxidation, we propose a catalytic site model at the catalyst surface (Fig. 11), involving Au^0 sites at the Au/ZnO interface and surface Au^{3+} site in proximity to Au^0. A bifunctional catalytic site consisting of adjacent Au^0 and Au^{3+} (Au^0–Au^{3+}) can be developed, which would facilitate the particulate matter oxidation according to a Langmuir-Hinshelwood reaction mechanism, involving the following steps:

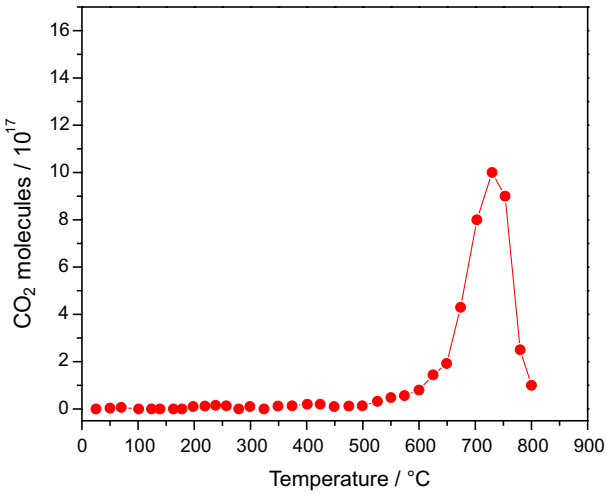

Fig. 10. Evolution of CO_2 as a function of temperature during particulate matter oxidation over quartz wool.

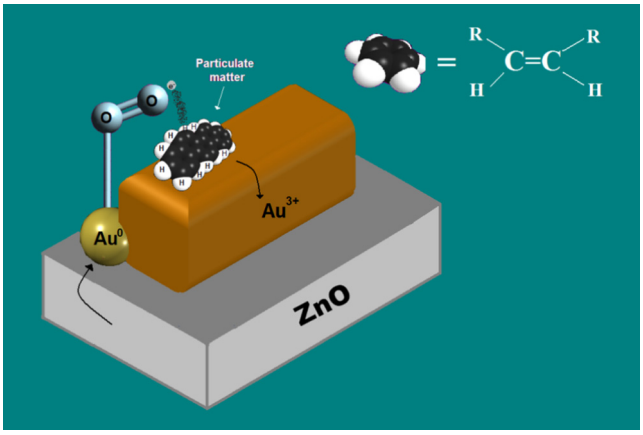

Fig. 11. Schematic model proposed to explain the high activity of 1%Au/ZnO for particulate matter oxidation.

1. Adsorption of O_2 on the Au^0 moiety (at the Au/ZnO interface) and generation of superoxide ions ($O_2^{\&-}$), the very active species well known for improving the oxidation of diesel particulate matter [65,66].
2. Simultaneous adsorption of particulate matter at the Au^{3+} moiety of the catalytic site. Adsorption may take place by the donation of the π electrons of the C=C bonds present in the particulates to Au^{3+} and π-back donation of *d* electrons of Au^{3+} to antibonding π^* orbitals of C=C.
3. Reaction of H—C bond of the adsorbed particulate matter molecule at Au^{3+} with the superoxide formed at Au^0, resulting in the abstraction of H atom by superoxide ion.

The simultaneous interaction between the adsorbed particulate matter on Au^{3+} with the superoxides formed on Au^0 would strongly increase the probability of particulate matter oxidation, resulting in the generation of CO_2 and H_2O molecules (as the final products) at very low oxidation temperature.

The results obtained in this investigation for 1%Au/ZnO were compared with the DPM oxidation performances of other group-IB metals supported on ZnO, such as 5%Cu/ZnO [67] and 3%Ag/ZnO (unpublished results) under similar experimental conditions. Obtained results indicate that the performance of metal-semiconductor catalysts depends on the electronic interactions at metal-semiconductor interface. The very high activity of 5%Cu/ZnO detected for this reaction can be explained considering the presence of the high active species Cu^{1+} at the metal-support interface, which might have been stabilized by the isoelectronic interaction between Zn^{2+} and Cu^{1+} at the interface. On the other hand, 3% Ag/ZnO did not present activity for DPM oxidation. XPS analysis performed on this catalyst revealed the presence of stable Ag^{1+} species, which is not active for this reaction. As the work function of Ag (4.26 eV) is lower than that of ZnO (~4.5 eV), an electronic transfer might have occurred form Ag to ZnO at the Ag/ZnO interface, increasing the stability of Ag^{1+}.

The simple preparation method, high activity, low T_{max}, and high stability of the Au nanoparticles in diesel particulate matter oxidation presented in this study might lead to its utilization as the part of commercial catalytic converter for diesel engines, despite the price of gold is currently a bit higher than the price of Pd, Pt or Rh, which are commonly used as active species for diesel emission abatement.

4. Conclusions

In summary, we demonstrated the high particulate matter oxidation capacity of hydrogen-reduced-air-calcined 1%Au/ZnO catalyst at very low temperature. The results obtained from diesel particulate matter oxidation behavior and electronic state analysis of incorporated gold in the catalyst suggest the formation of highly stable bifunctional Au^0–Au^{3+} catalytic surface sites which promote the contact efficiency of the solid particulate matter with the catalyst. While the Au^{3+} moieties enhance this contact efficiency, the Au^0 moieties enhance the generation of superoxide species at the gold-ZnO interface. Enhancement of contact efficiency of particulate matter at the catalyst surface and enhanced generation of superoxide species result in a high particulate matter oxidation activity for the gold loaded ZnO catalyst after annealing in hydrogen atmosphere. The high diesel particulate matter oxidation activity and high stability of the 1%Au/ZnO catalyst presented in this investigation show that the electronic state of gold and its electronic interactions with ZnO (n-type semiconductor) support surface are the key factors in diesel particulate matter oxidation.

Acknowledgments

The authors acknowledge VIEP & DITCo, BUAP, and SENER-CONACyT (Cluster Biodiesel 250014), Mexico, for their financial supports.

References

[1] M. Knauer, M.E. Schuster, D. Su, R. Schlogl, R. Niessner, N.P. Ivleva, J. Phys. Chem. A 113 (2009) 13871–13880.
[2] B.A.A.L. Van Setten, M. Makkee, J.A. Moulijn, Catal. Rev. 43 (2001) 489–564.
[3] M.V. Twigg, Appl. Catal. B 70 (2007) 2–15.
[4] I. Atribak, A. Bueno-López, A. García-García, Combust. Flame 157 (2010) 2086–2094.
[5] D. Fino, V. Specchia, Powder Technol. 180 (2008) 64–73.
[6] R. Allansson, P. Blakeman, B. Cooper, H. Hess, P.J. Silcock, A.R. Walker, SAE Technical Paper 2002-01-0428, 2002.
[7] W.F. Shangguan, Y. Teraoka, S. Kagawa, Appl. Catal. B 16 (1998) 149–154.
[8] A. Bueno-López, Appl. Catal. B 146 (2014) 1–11.
[9] J. Oi-Uchisawa, A. Obuchi, R. Enomoto, J. Xu, T. Nanba, S. Liu, S. Kushiyama, Appl. Catal. B 32 (2001) 257–268.
[10] K. Krishna, A. Bueno-Lopez, M. Makkee, J.A. Moulijn, Appl. Catal. B 75 (2007) 201–209.
[11] D. Fino, E. Cauda, D. Mescia, N. Russo, G. Saracco, V. Specchia, Catal. Today 119 (2007) 257–261.
[12] R. Cousin, S. Capelle, E. Abi-Aad, D. Courcot, A. Aboukaïs, Appl. Catal. B 70 (2007) 247–253.
[13] J.L. Hueso, A. Caballero, M. Ocaña, A.R. González-Elipe, J. Catal. 257 (2008) 334–344.
[14] Z. Zhang, Y. Zhang, Z. Wang, X. Gao, J. Catal. 271 (2010) 12–21.
[15] Y. Wei, Z. Zhao, T. Li, J. Liu, A. Duan, G. Jiang, Appl. Catal. B 146 (2014) 57–70.

[16] X.D. Wu, F. Lin, H.B. Xu, D. Weng, Appl. Catal. B 96 (2010) 101–109.
[17] X. Guo, M. Meng, F. Dai, Q. Li, Z. Zhang, Z. Jiang, S. Zhang, Y. Huang, Appl. Catal. B 142–143 (2013) 278–289.
[18] G. Bond, D.T. Thomson, Catal. Rev. Sci. Eng. 41 (1999) 319–388.
[19] M. Valden, X. Lai, D.W. Goodman, Science 281 (1988) 1647–1650.
[20] R. Kubo, J. Phys. Soc. Jpn. 17 (1962) 975–986.
[21] G.J. Hutchings, J. Catal. 96 (1985) 292–295.
[22] M. Haruta, T. Kobayashi, H. Sano, N. Yamada, Chem. Lett. 16 (1987) 405–408.
[23] C.Y. Ma, Z. Mu, J.J. Li, Y.G. Jin, J. Cheng, G.Q. Lu, Z.P. Hao, S.Z. Qiao, J. Am. Chem. Soc. 132 (2010) 2608–2613.
[24] Y. Wei, J. Liu, Z. Zhao, A. Duan, G. Jiang, C. Xu, J. Gao, H. He, X. Wang, Energy Environ. Sci. 4 (2011) 2959–2970.
[25] Y. Wei, J. Liu, Z. Zhao, Y. Chen, C. Xu, A. Duan, G. Jiang, H. He, Angew. Chem. Int. Ed. 50 (2011) 2326–2329.
[26] Y. Wei, J. Liu, Z. Zhao, A. Duan, G. Jiang, J. Catal. 287 (2012) 13–29.
[27] J.A. Hernández, G. Gómez, B. Pawelec, T.A. Zepeda, Appl. Catal. B 89 (2009) 128–136.
[28] A. Beck, A. Horváth, Gy. Stefler, R. Katona, O. Geszti, Gy. Tolnai, L.F. Liotta, L. Guczi, Catal. Today 139 (2008) 180–187.
[29] O. Pozdnyakova-Tellinger, D. Teschner, A. Wootsch, J. Kröhnert, B. Steinhauer, H. Sauer, L. Toth, F.C. Jentoft, A. Knop-Gericke, Z. Paál, R. Schlögl, J. Catal. 237 (2006) 1–16.
[30] D. Teschner, A. Wootsch, O. Pozdnyakova-Tellinger, J. Kröhnert, E. Vass, M. Hävecker, S. Zafeiratos, P. Schnörch, F.C. Jentoft, A. Knop-Gericke, R. Schlögl, J. Catal. 249 (2007) 318–327.
[31] M. Bandyopadhyay, O. Korsak, M.W.E. van den Berg, W. Grünert, A. Birkner, W. Li, F. Schüth, H. Gies, Micropor. Mesopor. Mater. 89 (2006) 158–163.
[32] M. Ruszel, B. Grzybowska, M. Łaniecki, M. Wójtowski, Catal. Commun. 8 (2007) 1284–1286.
[33] A.S.K. Hashmi, G.J. Hutchings, Angew. Chem. Int. Ed. 45 (2006) 7896–7936.
[34] A.I. Kozlov, A.P. Kozlova, H. Liu, Y. Iwasawa, Appl. Catal. A 182 (1999) 9–28.
[35] M. Haruta, N. Yamada, T. Kobayashi, S. Iijima, J. Catal. 115 (1989) 301–309.
[36] M.S. Chen, D.W. Goodman, Chem. Soc. Rev. 37 (2008) 1860–1870.
[37] M. Kotobuki, R. Leppelt, D.A. Hansgen, D. Widmann, R.J. Behm, J. Catal. 264 (2009) 67–76.
[38] N. Weiher, E. Bus, L. Delannoy, C. Louis, D.E. Ramaker, J.T. Miller, J.A. Van Bokhoven, J. Catal. 240 (2006) 100–107.
[39] C.J. Jia, Y. Liu, H. Bongard, F. Schth, J. Am. Chem. Soc. 132 (2010) 1520–1522.
[40] C. Harding, V. Habibpour, S. Kunz, A.N. Farnbacher, U. Heiz, B. Yoon, U. Landman, J. Am. Chem. Soc. 131 (2009) 538–548.
[41] G. Renaud, R. Lazzari, C. Revenant, A. Barbier, M. Noblet, O. Ulrich, F. Leroy, J. Jupille, Y. Borensztein, C.R. Henry, J. Deville, F. Scheurer, J. Mane-Mane, O. Fruchart, Science 300 (2003) 1416–1419.
[42] A. Caballero, J.P. Holgado, V.M. Gonzalez-delaCruz, S.E. Habas, T. Herranz, M. Salmeron, Chem. Commun. 46 (2010) 1097–1099.
[43] T. Schalow, M. Laurin, B. Brandt, Angew. Chem. Int. Ed. 44 (2005) 7601–7605.
[44] Y. Wei, Z. Zhao, X. Yu, B. Jin, J. Liu, C. Xu, A. Duan, G. Jiang, S. Ma, Catal. Sci. Technol. 3 (2013) 2958–2970.
[45] K.L. Fujdala, T.J. Truex, J. Jia, US Patent 7 745 367, Nanostellar, Inc., 2010.
[46] B.R. Stanmore, J.F. Brilhac, P. Gilot, Carbon 39 (2001) 2247–2268.
[47] K. Villani, C.E.A. Kirschhock, D. Liang, G.V. Tendeloo, J.A. Martens, Angew. Chem. Int. Ed. 45 (2006) 3106–3109.
[48] R. Kimura, J. Wakabayashi, S.P. Elangovan, M. Ogura, T. Okubo, J. Am. Chem. Soc. 130 (2008) 12844–12845.
[49] J. Oi-Uchisawa, S. Wang, T. Nanba, A. Ohi, A. Obuchi, Appl. Catal. B 44 (2003) 207–215.
[50] F.E. López-Suárez, A. Bueno-López, M.J. Illán-Gómez, Appl. Catal. B 84 (2008) 651–658.
[51] I. Atribak, A. Bueno-López, A. García-García, P. Navarro, D. Frías, M. Montes, Appl. Catal. B 93 (2010) 267–273.
[52] K. Yamasaki, T. Kayama, F. Dong, H. Shinjoh, J. Catal. 282 (2011) 289–298.
[53] Y. Wei, Z. Zhao, J. Liu, S. Liu, C. Xu, A. DUan, G. Jiang, J. Catal. 317 (2014) 62–74.
[54] H. Ranji-Burachaloo, S. Masoomi-Godarzi, A.A. Khodadadi, Appl. Catal. B 182 (2016) 74–84.
[55] T. Nanba, S. Masukawa, A. Abe, J. Uchisawa, A. Obuchi, Appl. Catal. B 123–124 (2012) 351–356.
[56] M. Piumetti, S. Bensaid, N. Russo, D. Fino, Appl. Catal. B 165 (2015) 742–751.
[57] J.P.A. Neeft, O.P. Van Pruissen, M. Makkee, J.A. Moulijn, Appl. Catal. B 12 (1997) 21–31.
[58] E. Kowalska, O.O.P. Mahaney, R. Abe, B. Ohtani, Phys. Chem. Chem. Phys. 12 (2010) 2344–2355.
[59] Y. Hu, H.J. Chen, J. Nanopart. Res. 10 (2008) 401–407.
[60] G.M. Veith, A.R. Lupine, S. Rashkeev, S.J. Pennycook, D.R. Mullins, V. Schwartz, C.A. Bridges, N.J. Dudney, J. Catal. 262 (2009) 92–101.
[61] A. Goguet, R. Burch, Y. Chen, C. Hardacre, P. Hu, R.W. Joyner, F.C. Meunier, B.S. Mun, D. Thompserr, D. Tibiletti, J. Phys. Chem. C 111 (2007) 16927–16933.
[62] M. Salamanca, F. Mondragon, J.R. Agudelo, P. Benjumea, A. Santamaria, Combust. Flame 159 (2012) 1100–1108.
[63] L.J. Bellamy, The Infrared Spectra of Complex Molecules, Chapman and Hall, London, 1975.
[64] Z. Sarbak, Appl. Catal. A 177 (1999) 85–97.
[65] K. Villani, R. Brosius, J.A. Martens, J. Catal. 236 (2005) 172–181.
[66] E. Aneggi, J. Llorca, C. Leitenburg, G. Dolcetti, A. Trovarelli, Appl. Catal. B 91 (2009) 489–497.
[67] G. Corro, S. Cebada, U. Pal, J.L. García Fierro, Appl. Catal. B 165 (2015) 555–565.